CrossMark

Low-temperature synthesis of hexagonal barium ferrite (BaFe$_{12}$O$_{19}$) nanoparticles by annealing at 450 °C followed by quenching

A structural, thermokinetic, magnetic and photoluminescence study

Ranjit K. Verma[1,2] · **Rakesh K. Singh[3]** · **A. Narayan[4]** · **Lata Verma[1]** ·
Amrendra K. Singh[1] · **Anit Kumar[1]** · **Pankaj K. Pathak[1]** · **Abhay K. Aman[3]**

Abstract Citrate precursor method has been used to obtain nanosized particles of barium hexaferrite at low temperatures. Samples were annealed at 450 °C for 3 and 5 h. Quenching of the third sample was done by taking the crucible out from the muffle furnace after annealing it for 5 h and putting it abruptly into an ice bath. The saturation magnetization has been found to be 4.36 and 0.04 emu g^{-1} for the samples obtained upon annealing at 450 °C for 3 and 5 h, respectively, while that of the quenched sample has been found to be 4.61 emu g^{-1}. In case of the sample obtained after 5-h annealing, the squareness value was found to be maximum indicating significance in memory and switching applications. For the quenched and the 3-h annealing products, the magnetic data values are similar. Creation of spin disorders on the surface upon prolonged annealing, due to disappearance of oxygen ions and subsequent breakage of superexchange interactions between cations, has been undone upon quenching. The XRD and TEM data indicate that the particle size (9–17 nm) gets lower in case of the quenched samples. Photoluminescence study of the quenched sample furnished prominent peaks in UV, visible and near-IR regions under 200-nm excitation. The TG–DSC data were analysed for the kinetic parameters, activation energy (E), pre-exponential factor (A) using the Kissinger isoconversion and the Ozawa–Flynn–Wall methods for the first-step decomposition of the quenched sample.

Keywords TG–DSC studies · Dehydrated gel · Thermal quenching · Barium ferrite · Nanoparticles · Coercivity · Magnetization · Thermal stability · Photoluminescence

✉ Ranjit K. Verma
profrkverma@gmail.com

1 University Department of Chemistry (DST-FIST Sponsored and UGC-BSR Supported), Magadh University, Bodh Gaya 824 234, India

2 Patna University, Patna 800 005, India

3 Aryabhatta Centre for Nanoscience and Nanotechnology, Aryabhatta Knowledge University, Patna 800 001, India

4 University Department of Physics, Patna University, Patna 800 005, India

Introduction

The hexaferrites are interesting ferrimagnetic materials. These ferrites have hexagonal crystal structure, and they have always been among technologically and commercially most exciting materials/substances. These are hard, have better high-frequency magnetic properties [1] and are known for their magnetic anisotropy which is larger than that of the series of the spinel group. They are being used in MW/GHz electronic components, radar-absorbing materials and variety of materials having magnetoelectric/multiferroic applications. As an example, barium hexaferrites (BaFe$_{12}$O$_{19}$–denoted as BaM) can be considered. These are among uniaxial M-ferrites with high magnetic saturation (M_s) and high coercivity (H_c) values [2–5]. Their hexagonal structure is of magnetoplumbite type (space group P6$_3$/mmc). It consists of alternate hexagonal and spinel blocks bringing similarity in structure with both garnet and spinel ferrites [6]. It has many unique features besides being a low-cost material with high magnetic anisotropy and remarkable corrosion resistivity. Its application as permanent magnet and its use in recording media, microwave

filters and magneto-optic materials give it prominence. Fields such as electromagnetic interference and electromagnetic radiation pollution are incomplete without BaM. They are wonderful microwave absorbers [7].

Like in other cases, barium ferrites too can be synthesized by citrate precursor, sol–gel, chemical coprecipitation, hydrothermal, glass crystallization and microemulsion methods [6]. Substitutions have also been tried successfully to study its impact on its applications [8, 9]. The effect of crystallinity and particle morphology of the submicron barium hexaferrite ($BaFe_{12}O_{19}$) powders on the magnetic properties was investigated on powders synthesized by different methods [10]. The properties of nanomaterials, their particle size, etc., vary significantly with the methodology adopted for their preparations. This, in turn, affects their application potentialities [11]. For optimizing the annealing/sintering temperature, it has been observed that the loss of water and curing of the precursor can be optimized by 450 °C in cases of aluminates, chromites and cobalt ferrites [11–13].

In fact, the data obtained from the TG and DSC techniques and the kinetic and mechanistic analysis of those data have more frequently been used to study the thermal behaviour of materials. These facilitate understanding of the thermodynamics and kinetics of various transformations including phase changes that take place under a dynamic heating programme [14–24], and this way, we can understand curing in a more meaningful way as in cases of the precursors mentioned above. In the present case, the TG–DSC techniques have been applied to observe changes in thermal behaviour with change in the period for which the sample was annealed.

Usually, barium hexaferrites are much more difficult to prepare than spinel ferrites as higher temperatures or pressures are required and the reaction takes much time. At higher temperatures, required formation of γ-Fe_2O_3 is disfavoured and formation of α-Fe_2O_3 takes place [6]. In this work, we have used very low temperature to synthesize barium hexaferrite nanoparticles using chemical-based citrate precursor method. By varying the annealing time, significant magnetic properties have been observed in particles obtained by annealing for 3 h and in a repetition, the 5-h annealing has been followed by quenching. The thermal, XRD, TEM, photoluminescence and magnetic study data indicate its significant application potentialities.

Experimental

Materials

Nanosized samples of barium hexaferrite powder were synthesized by the citrate precursor method. The starting compounds, ferric nitrate, barium nitrate and citric acid (AR), were taken in stoichiometric proportion, and their respective aqueous solutions (in minimum quantities of deionized water) were prepared. Stirring constantly, solutions of the salts were mixed together. This was followed by addition of the citric acid solution. The mixture was heated to temperature between 60 and 80 °C for 2 h with continuous stirring, and after that, it was allowed to cool to room temperature and to dry overnight in air oven at 90–95 °C to obtain the dehydrated precursor which was a brown fluffy powder. Three samples of the ferrites were obtained by heating this precursor at 450 °C for 1, 3 and 5 h, respectively, in a muffle furnace. Quenching of the third sample (annealed for 5 h) was done by taking the crucible out from the muffle furnace and putting it abruptly into an ice bath.

Methods

The three samples were subjected to TG–DSC analysis on TG–DSC1 (Mettler) using STAR under dynamic heating programmes (5°/10°/15 °C min^{-1}) under O_2 and N_2 purging. Thermal curves (TG–DSC) of the quenched sample were recorded under four heating rates (5°/10°/20°/50 °C min^{-1}) for kinetic analysis. The powders were characterized using X-ray diffractometer [XRD Model D/max-IIB, Rigaku, with CuKα radiation source ($\lambda = 1.5418$ Å) operating in the Bragg–Brentano geometry in a 2θ range of 10.0°–80.0° at a scan step of 0.020° and scan rate of 20/min] for phase and particle size. Particle size estimation was done using Scherrer formula ($d = 0.9\lambda/\beta \, Cos\theta$). It was followed by transmission electron microscopy. Magnetic measurements were taken on a vibrating sample magnetometer (VSM, PAR155). The photoluminescence of the quenched sample was measured on a fluorescence spectrometer LS-55 (PerkinElmer) at room temperature in the wavelength range of 200–900 nm using excitation wavelength source of 200 nm.

Results and discussion

X-ray diffraction analysis

The X-ray diffraction spectra of the synthesized materials are shown in Fig. 1. Maximum intensity peaks have been selected for particle size calculation, and using Scherrer formula ($d = 0.9\lambda/\beta \, Cos\theta$), the particle sizes were found to be 40 and 43 nm in cases of particles obtained by annealing for 3 and 5 h, respectively (Table 1). Annealing time promotes increase in particle size. But quenched sample shows poor crystallinity with crystallite size of 30 nm. All samples show hexagonal structure as per the ICDD/JCPDS database (No-190098 and 78-0135). Particle size,
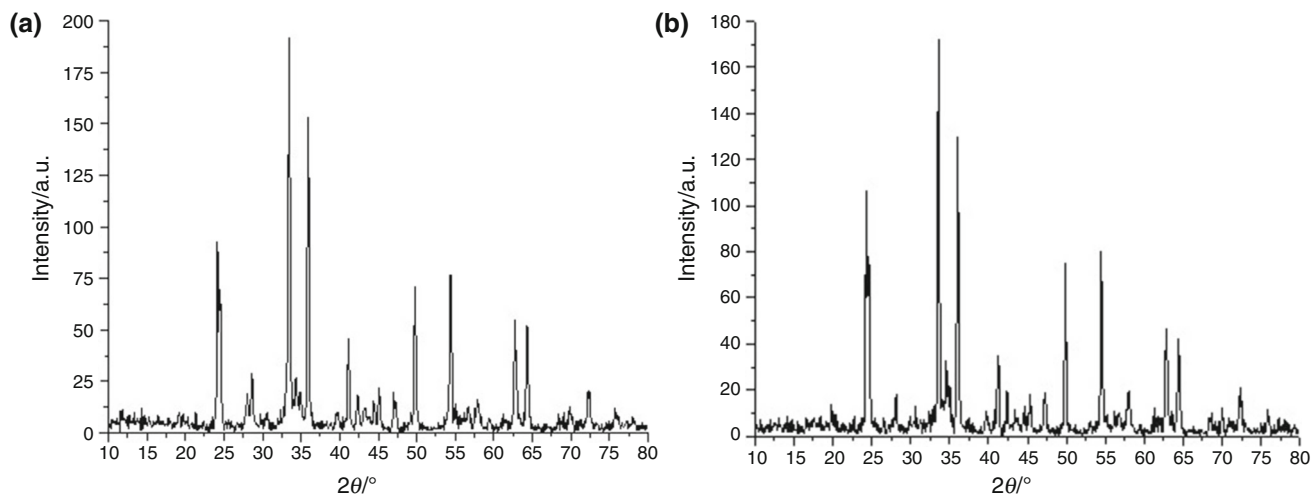
Fig. 1 **a** XRD curve of the samples obtained after annealing for 5 h. **b** XRD curve of the quenched sample

Table 1 XRD data of the barium ferrite samples prepared under different modes

| Preparatory mode	XRD peak position/°	Peak intensity height/cps	Interplanar spacing/Å	Particle size/nm
3-h annealing	33.345	567	2.686	40
5-h annealing	33.558	477	2.674	43
5-h annealing followed by quenching	33.483	353	2.668	30

interplanar distance (d) and prominent peak intensity height are lower as compared to those of samples prepared by other methods. In the preparation of hexaferrites, higher annealing temperature is required to obtain pure phase. This results in significant increase in particle size as well as improvement of ion occupancy [25]. Upon quenching, the intensity of the prominent peaks is lower. The decrease in the crystallite size upon quenching is quite evident and can be considered as a good indicator of moderate crystallinity and better chemical homogeneity. The XRD peak positions of the prepared samples thus indicate the presence of $BaFe_{12}O_{19}$ as major phase. Some small peaks of very small intensities are due to the presence of $BaCO_3$, γ-Fe_2O_3 and $BaFe_2O_4$. Annealing and quenching at different temperatures generally facilitate solid-state diffusion of BaO and Fe_2O_3, and this leads to the conversion of the raw materials into the hexaferrite and spinel phases. During annealing, some Ba^{2+} might be reacting with γ- or α-Fe_2O_3 to form barium monoferrite ($BaFe_2O_4$) which in turn may be yielding barium hexaferrite by combining with oxide materials (γ- or α-Fe_2O_3).

Transmission electron microscopy

The TEM pictures of the 5-h samples (unquenched/quenched) are shown in Fig. 2a–e. The particle size (9–17 nm) is lower in case of the quenched samples.

Thermal analysis

TG–DSC curves of all the three annealed samples, recorded under O_2 and N_2 purging, have similar features. The first peak is a sharp exopeak, and the peak temperature comes around 150 °C (Fig. 3). Though small, the second peak comes during the second step of decomposition. As expected, the curing curve which follows the second step becomes broadened and prominent under O_2 purging indicating enhanced oxidation. It is complete well before 350 °C, and the 5-hour curing seems to be heading for complete curing around this temperature. The TG–DSC curves (N_2 purging) of the sample annealed for 5 h followed by quenching are shown in Fig. 4. In all the cases, the peak has been found to be shifting towards higher temperature with increase in the heating rate, though the process starts taking place earlier indicating lesser thermal stability at higher heating rate. The peak widening is also observed with this increase. The TG–DSC data (Table 2) were analysed for the kinetic parameters, activation energy (E), pre-exponential factor (A) using the Kissinger iso-conversion [26, 27] and the Ozawa–Flynn–Wall [28, 29] methods for the first-step decomposition of the quenched sample, and the values are presented in Table 3. Values of the activation entropy, $\Delta S^{\#}$, were also approximated using Eqs. (1–5):
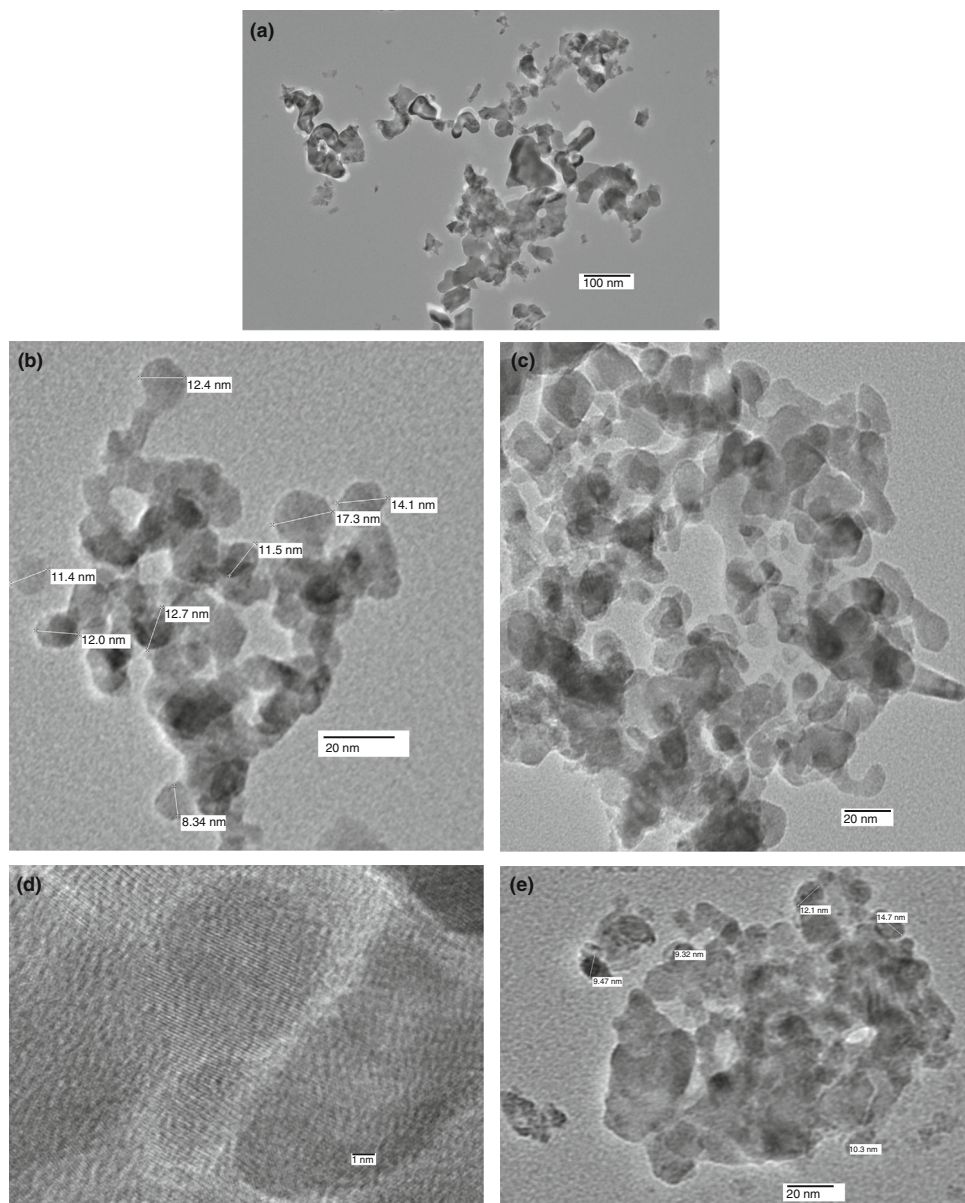
Fig. 2 a–e TEM pictures of 5-h samples (unquenched/quenched)

- Kissinger equation:

$$\ln\left(\beta/T_m^2\right) = -E/RT_m + \ln(AR/E) \qquad (1)$$

where β = heating rate, T_m = peak temperature and R = gas constant. Plotting $\{\ln(\beta/T_m^2)$ *vs.* E/RT_m furnished a straight line, and the resultant slope and the intercept were used for the values of E and $A\}$.

- Ozawa–Flynn–Wall equation:

$$\ln(\beta) = \text{constant} - 1.052E/RT_m \qquad (2)$$

- $$\Delta S^{\#} = R \ln Ah/kT \qquad (3)$$

where k is the Boltzmann constant and the temperature T is taken as T_m instead of T at $\alpha = 0.5$ as has been the usual practice [13], since T_m seems to be more convincing point as it has been found to be yielding more coherent results (Table 2).
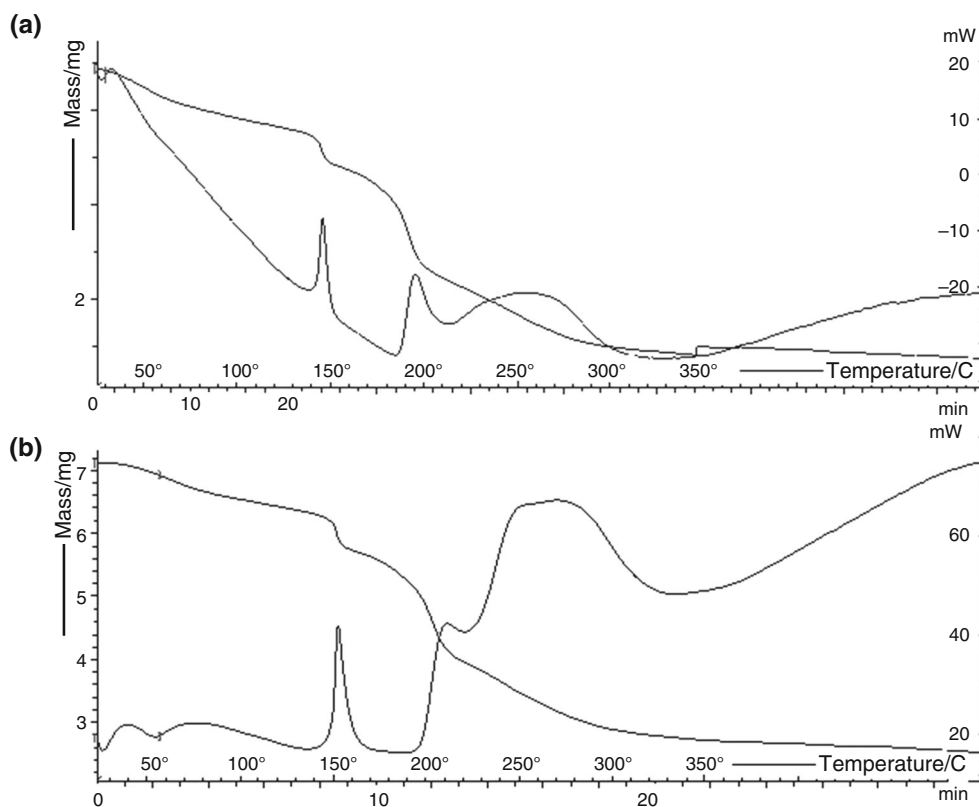
- $$\Delta H^{\#} = \Delta E^{\#} - RT \qquad (4)$$

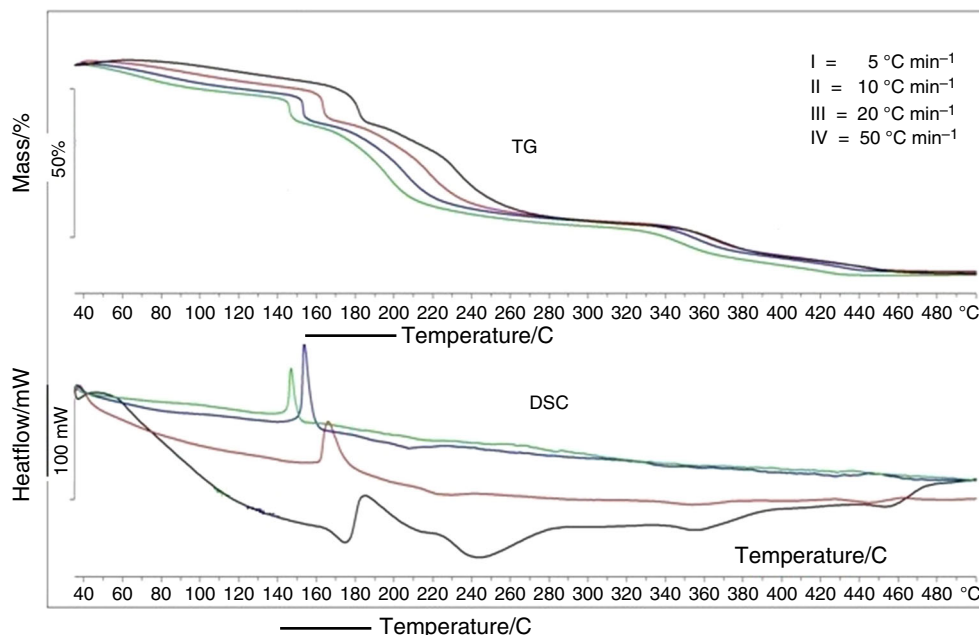- $$\Delta G^{\#} = \Delta H^{\#} - T\Delta S^{\#} \qquad (5)$$

where G is the Gibbs free energy and H, the enthalpy.

Fig. 3 TG–DSC curves of annealed sample

Fig. 4 TG–DSC curves of the quenched sample under different heating rates

Magnetic measurement

The magnetization curves of BaFe₁₂O₁₉ hexaferrite nanoparticles obtained upon annealing for 3 and 5 h and that after quenching are shown in Fig. 5. Their magnetic parameters, viz., magnetization, coercivity, retentivity and squareness, are presented in Table 4. The saturation magnetization has been found to be 4.36 and 0.04 emu/g, respectively, for samples obtained upon annealing at 450 °C for 3 and 5 h, respectively, while that of the quenched sample has been found to be 4.61 emu g⁻¹. Since the saturation magnetization for bulk of barium

Table 2 TG–DSC data of the barium ferrite nanoparticles obtained after quenching*

Heating rate/deg/min	$\beta = 5$		$\beta = 10$		$\beta = 20$		$\beta = 50$	
	TG	DSC peak, $T_m/T_{0.5}$	TG	DSC peak, $T_m/T_{0.5}$	TG	DSC peak, $T_m/T_{0.5}$	TG	DSC peak, $T_m/T_{0.5}$
% loss, two steps	20.75/34.68	–	20.52/39.17	–	20.22/39.91	–	21.0/41.82	–
Temperature range of the first step/C	37.7–150.1/158.4–223.5	146.28/113.2	39.1–161.3/164.3–278.9	153.05/123.7	41.7–167.1/170.6–287.6	163.6/138.7	54.5–182.0/185.4–322.5	183.62/162.5

* $T_{0.5}$ = temperature corresponding to $\alpha = 0.5$

hexaferrite nanoparticles has been reported in the range of 50 emu g^{-1} [29–31], an evident lowering is there which shows that the magnetization values are reduced drastically in nanoscale. Magnetic nanomaterials can conveniently be understood by dividing into core region of ordered spin arrangement and a surface or shell region with structural and spin disorder [32]. Reduced magnetization indicates that the spins are less ordered in such nanoparticles. Creation of such disorder may be due to disappearance of oxygen ions and subsequent breakage of superexchange interactions between cations [33]. This happens more at the surface. The spin disorders do also lead to a rise in the coercivity. Thus, the change in the particle size favours spin disorder and subsequent decrease in magnetization. The squareness ratio is especially important in memory and switching application areas. In case of the sample obtained after 5-h annealing, the squareness value was found to be maximum. For the quenched and the 3-h annealing product, the values are similar. These values indicate that the creation of the spin disorders on the surface that is apparently happening upon prolonged annealing, is being undone upon quenching.

The rise in the annealing hours and quenching of the samples possibly result in spin disorder to some extent. This may be the cause of lower magnetization which may be considered as an evidence of occurrence of spin disorder.

Photoluminescence studies

Ferrites [11] have been found to be furnishing interesting and useful peaks in the photoluminescence (PL) spectrum. The PL study of the quenched sample under study furnished prominent peaks in UV, visible and near-IR regions under 200-nm excitation (Fig. 6; Table 5).

Photoluminescence is the emission of light from a material which is stimulated by input of energy, and it occurs when the radiative relaxation occurs. The density of electrons excited by the incident photons and the holes and hence the peak intensity are controlled by the excitation wavelength. Besides, the maximum peak intensity does correspond to the maximum transition probability. These emissions may be due to the transition of excited optical centres present in the inside electronic levels of the synthesized hexaferrite magnetic nanoparticles [34]. In this case, the oxygen vacancies are most common defects. These may act as the radiative centres in the luminescence processes under discussion. The peaks around 3 eV are mainly due to quantum confinement. The quantum confinement phenomenon could be used to explain the mechanism. Like in the case of cobalt ferrites [11], there may be shortening of the superexchange interaction bond length. This shortening is bound to result

Table 3 Kinetic parameters*

Sl. no.	Method				
E/kJ mol^{-1}	Ozawa–Flynn–Wall	61.15			
	Kissinger	73.16, *68.24*			
ln$A$	Ozawa–Flynn–Wall	17.63			
	Kissinger	16.52, *16.66*			
Heating rate/deg min^{-1}		$\beta = 5$	$\beta = 10$	$\beta = 20$	$\beta = 50$
$T_m(T_{0.5})$/K		420.04, *386.17*	427.41, *396.71*	439.66, *411.69*	460.14, *435.48*
$\Delta S^{\#}$/J K^{-1} mol^{-1}	Ozawa–Flynn–Wall	−100.505	−100.728	−101.036	−101.504
	Kissinger	−109.71, *−109.26*	−109.934, *−109.401*	−110.242, *−109.636*	−110.709, *−110.015*
ΔH/kJ mol^{-1}	Ozawa–Flynn–Wall	57.94	57.85	57.73	57.53
	Kissinger	−100.34, *−108.09*	−101.22, *−108.70*	−102.47, *−109.72*	−104.45, *−111.42*
ΔG/kJ mol^{-1}	Ozawa–Flynn–Wall	96.75	97.81	99.32	101.73
	Kissinger	32.33, *35.08*	33.49, *35.89*	35.14, *37.23*	37.77, *39.48*

* values in italics denote values corresponding to $T_{0.5}$
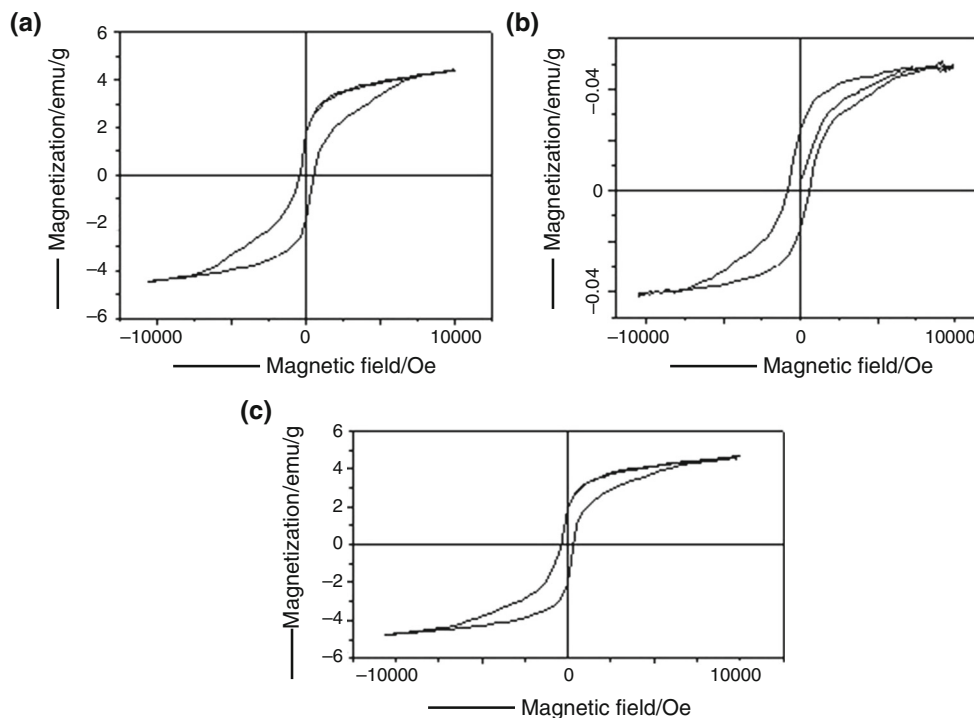
Fig. 5 Magnetization curves of the annealed sample for **a** 3 h, **b** 5 h and that **c** of the quenched sample

in changes in the electronic structures. As we have earlier pointed out, there may also be participative non-radiative relaxation channels at the surface. Applying the Fermi golden rule of quantum mechanics [35], the transition probability is significant only when $h\nu = \Delta E$ or $\lambda = hc/\Delta E$ (where λ is the wavelength of the radiation and ΔE is the gap between the electronic energy states). Therefore, in the observed emission spectra widely varied peaks in the ranges, UV, visible and near-IR, are due to the dependence upon the individual vibrational energy levels of the ground and excited states and superexchange interaction [36] in the barium hexaferrite nanoparticles prepared. As in the case of cobalt ferrites [11], the phenomenon could also be understood further in terms of Stokes shift between the absorption surface defects and surface defects.

Table 4 Magnetic parameters of the three samples of barium ferrite

Annealing hours	Saturation magnetization/ emu g^{-1}	Coercivity/ Oe	Retentivity/ emu g^{-1}	Squareness/retentivity/saturation magnetization
3 h	4.36	438.70	1.66	0.38
5 h	0.04	835.12	0.023	0.57
5 h followed by quenching	4.61	355.58	1.79	0.39

Fig. 6 Photoluminescence curve of the quenched sample
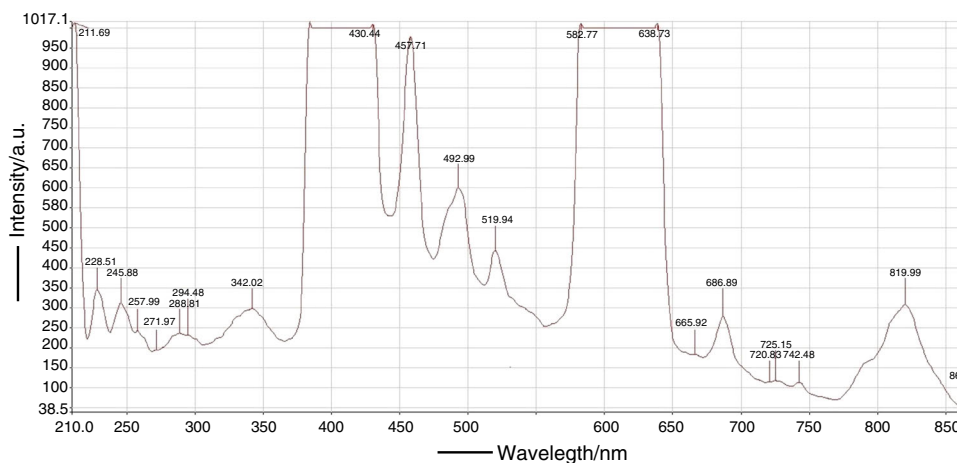
Table 5 Peak values in nm in the photoluminescence spectrum of the quenched sample*

UV region	Visible region	Near-IR region
228.51/*5.435*, 245.88/*5.05*, 257.99/*4.814*, 288.81/*4.30*, 294.48/*4.217*,342.02/*3.631*	457.71/*2.71*, 492.99/*2.52*,519.94/*2.388*, 663.92/*1.87*, 686.89/*1.81*	720.83/*1.72*,725.15/*1.71*, 742.48/ *1.67*, 819.99/*1.51*

* values in italics are in eV

Conclusion

- Nanosized particles (9–17 nm) of barium hexaferrite have been obtained at low temperatures using citrate precursor method after 5-h annealing at 450 °C followed by temperature quenching. Annealing time promotes increased particle size, while quenching leads to reduction in the particle size.

- The XRD peak positions of the samples indicate the presence of $BaFe_{12}O_{19}$ as major phase. Some small peaks of very small intensities are due to the presence of $BaCO_3$, γ-Fe_2O_3 and $BaFe_2O_4$. This may be ascribed to the rise in the annealing hours and to the quenching of the samples—possibly resulting in spin disorder to some extent. This may be the cause of lower magnetization which may be considered as an evidence. Annealing and quenching at different temperatures generally facilitate solid-state diffusion of BaO and Fe_2O_3, and this leads to the conversion of the raw materials into the hexaferrite and spinel phases. During annealing, some Ba^{2+} might be reacting with γ- or α-Fe_2O_3 to form barium monoferrite ($BaFe_2O_4$) which in turn may be yielding barium hexaferrite by combining with oxide materials (γ- or α-Fe_2O_3).

- The saturation magnetization has been found to be 4.36 and 0.04 emu g^{-1} for the samples obtained upon annealing at 450 °C for 3 and 5 h, respectively, while that of the quenched sample has been found to be 4.61 emu/g.

- In case of the sample obtained after 5-h annealing, the squareness value was found to be maximum indicating significance in memory and switching applications.

- For the quenched and the 3-h annealing products, the magnetic data values are similar. Creation of spin disorders on the surface upon prolonged annealing, due to disappearance of oxygen ions and subsequent breakage of superexchange interactions between cations, is being undone upon quenching.

- Photoluminescence study of the quenched sample furnished prominent peaks in UV, visible and near-IR regions under 200-nm excitation.

References

1. Ri CH, Li L, Qi Y. Anisotropy of the electrical conductivity in W-type hexagonal ferrites BaFe$_{18}$O$_{27}$ and BaCo$_2$Fe$_{16}$O$_{27}$ from first principles. J Magn Magn Mater. 2012;324(8):1498–502.

2. Pullar RC, Bdikin IK, Bhattacharya AK. Magnetic properties of randomly oriented BaM, SrM, Co$_2$Y, Co$_2$Z and Co$_2$W hexagonal ferrite fibres. J Europ Cer Soc. 2012;32(4):905–13.

3. Campbell P. Permanent magnet materials and their application. Cambridge: Cambridge University Press; 1994.

4. Topal U, Ozkan H, Sozeri H. Synthesis and characterization of nanocrystalline BaFe12O19 obtained at 850 °C by using ammonium nitrate melt. J Magn Magn Mater. 2004;284:416–22.

5. Molaei MJ, Ataie A, Raygan S, Picken SJ, Tichelaar FD. The effect of heat treatment and re-calcination on magnetic properties of BaFe$_{12}$O$_{19}$/Fe$_3$O$_4$ nano-composite. Ceram Int. 2012;38(4):3155–9.

6. Liu Y, Drew MGB, Liu Y. Optimizing the methods of synthesis for barium hexagonal ferrite—An experimental and theoretical study. Mater Chem Phys. 2012;134:266–72.

7. Li CJ, Wang B, Wang JN. Magnetic and microwave absorbing properties of electrospun Ba$_{(1-x)}$La$_x$Fe$_{12}$O$_{19}$ nanofibers. J Magn Magn Mater. 2012;324(7):1305–11.

8. Chang S, Kangning S, Pengfei C. Microwave absorption properties of Ce-substituted M-type barium ferrite. J Magn Magn Mater. 2012;324(5):802–5.

9. Topal U. Towards further improvements of the magnetization parameters of B$_2$O$_3$-Doped BaFe$_{12}$O$_{19}$ particles: etching with hydrochloric acid. J Supercond Nov Magn. 2012;25:1485–8.

10. Dursun S, Topkaya R, Akdogan N, Alkoy S. Comparison of the structural and magnetic properties of submicron barium hexaferrite powders prepared by molten salt and solid state calcination routes. Ceram Int. 2012;38(5):3801–6.

11. Singh RK, Narayan A, Prasad K, Yadav RS, Pandey AC, Singh AK, Verma L, Verma RK. Structural, magnetic and photoluminescence studies on cobalt ferrite nanoparticles obtained by citrate precursor method. J Therm Anal Calorim. 2012;110:573–80.

12. Singh RK, Yadav A, Narayan A, Singh AK, Verma L, Verma RK. Thermal, structural and magnetic studies on chromite spinel, synthesized by citrate precursor method and annealed at temperature 450 °C and 650 °C. J Therm Anal Calorim. 2012;107:197–204.

13. Singh RK, Yadav A, Narayan A, Chandra M, Verma RK. Thermal, XRD and magnetization studies on ZnAl2O4 and NiAl2O4 spinels, synthesized by citrate precursor method and annealed at temperature 450 °C and 650 °C. J Therm Anal Calorim. 2012;107:205–10.

14. Verma RK, Hill JO, Niinisto L, Mojumdar SC, Kumar DD. A curriculum framework for education in thermal analysis. J Mater Educ. 2012;34:133–50.

15. Verma RK, Verma L, Chandra M. Thermoanalytical studies on the non-isothermal dehydration and decomposition of dl-lactates of a series of transition metals. Indian J Chem. 2003;42A:2982–7.

16. Bhattacharjee NC, Kumar M, Kumar S, Verma RK. Kinetic and mechanistic studies on non-isothermal decomposition of potassium dioxalatocuprate(II) dihydrate. J Indian Chem Soc. 1998;75(5):317–8.

17. Verma RK, Verma L, Chandra M, Bhushan A. Non-isothermal dehydration and decomposition of dl-lactates of transition metals and alkaline earth metals: a comparative study. J Therm AnalCalorim. 2005;80:351–4.

18. Kumar M, Verma RK, Verma L, Bhattacharjee NC, Kumar S, Verma BP. Thermal decomposition of potassium trioxalato chromate(III) trihydrate: a kinetic and mechanistic study. Asian J Chem. 1996;8(3):543–6.

19. Agrawal HL, Mishra A, Ambasta RK, Verma L, Verma RK, Verma BP. Kinetic parameters of thermolysis of complexes of rhodium(III), palladium(II) and platinum(II) with substituted morpholines from their non-isothermal thermogravimetric data. Asian J Chem. 1994;6:130–4.

20. Verma BP, Verma RK, Chandra M, Pandey S, Mallick AK, Verma L. A study of non-isothermal decomposition of calcium dl-lactate pentahydrate. Asian J Chem. 1994;6:606–12.

21. Verma RK, Verma L, Ranjan M, Verma BP, Mojumdar SC. Thermal analysis of 2-oxocyclopentanedithiocarboxylato complexes of iron(III), copper(II) and zinc(II) containing pyridine or morpholine as the second ligand. J Therm Anal Calorim. 2008;94:27–31.

22. Verma RK, Verma L, Bhushan A, Verma BP. Thermal decomposition of complexes of cadmium(II) and mercury(II) with triphenylphosphanes. J Therm Anal Calorim. 2007;90:725–9.

23. Brown ME, Gallagher PK. Introduction to recent advances, techniques and applications of thermal analysis and calorimetry. In: Brown ME, Gallagher PK, editors. Hand book of thermal-analysis and calorimetry. New York: Elsevier; 2008. p. 1–12.

24. Verma RK, Verma L, Chandra M, Verma BP. Kinetic parameters of thermal dehydration and decomposition from thermoanalytical curves of zinc dl-lactate. J Indian Chem Soc. 1998;75:162–4.

25. Wang J, Chen Q, Che S. Magnetic properties in BaFe$_{12}$O$_{19}$ nanoparticles prepared under a magnetic field. J Magn Magn Mater. 2004;280:281–6.

26. Kissinger HE. Variation of peak temperature with heating rate in differential thermal analysis. J Res Natl Bur Stand. 1956;57:217–21.

27. Kissinger HE. Reaction kinetics in differential thermal analysis. Anal Chem. 1957;29:1702–6.

28. Flynn JH, Wall LA. A quick, direct method for the determination of activation energy from thermogravimetric data. Polym Lett. 1966;4:323–8.

29. Ozawa T. A new method of analyzing thermogravimetric data. Bull Chem Soc Jpn. 1965;38:1881–6.

30. Wohlfarh EP. Fundamental properties of hexaferrite with magnetoplumbite structure in ferromagnetic materials. NewYork: North-Holland Publishing Company; 1982.

31. Martirosyan KS, Galstyan Hossain, Wang YJ, Litvinov D. Barium hexaferrite nanoparticles: synthesis and magnetic properties. Mater Sci Eng, B. 2011;176:8–13.

32. Kodama RH, Berkowitz AE, Mcniff EJ, Foner S. Surface disorder in NiFe$_2$O$_4$ nanoparticles. Phys Rev Lett. 1996;77:394–7.

33. Misra RDK, Gubbala S, Kale A. Egelhoff Jr WF.A comparison of the magnetic characteristics of nanocrystalline nickel, zinc, and manganese ferrites synthesized by reverse micelle technique. Mater Sci Eng, B. 2004;111(2–3):164–74.

34. Mishra DK, Qi X. Energy levels and photoluminescence properties of nickel-doped bismuth ferrite. J Alloys Compd. 2010;504:27–31.

35. Ghatak AK, Loknathan S. quantum mechanics, theory and applications. India: Macmillan India Ltd; 1984. p. 503.

36. Siwach OP, Sen P. Synthesis and study of fluorescence properties of Cu nanoparticles. J Nanopart Res. 2008;10:107–14.